

**MICRO-SEISMOMETERS VIA ADVANCED MESO-SCALE FABRICATION**

Caesar T. Garcia, Guclu Onaran, Brad Avenson, Matt R. Christensen, Zhizhi Liu, Nishshanka Hewa-Kasakarage,  
and Neal A. Hall

Silicon Audio

Sponsored by the National Nuclear Security Administration

Award No. DE-FG02-08ER85106

**ABSTRACT**

The Department of Energy (DOE) and the National Nuclear Security Administration (NNSA) seek revolutionary sensing innovations for the monitoring of nuclear detonations. Performance specifications are to be consistent with those obtainable by only an elite few products available today, but with orders of magnitude reduction in size, weight, power, and cost. The proposed commercial innovation calls upon several technologies including the combination of meso-scale fabrication and assembly, photonics-based displacement / motion detection methods, and the use of digital control electronics. Early Phase II development has demonstrated verified and repeatable sub 2ng noise floor from 3Hz to 100Hz, compact integration of 3-axis prototypes, and robust deployment exercises. Ongoing developments are focusing on low frequency challenges, low power consumption, ultra-miniature size, and low cross axis sensitivity. We are also addressing the rigorous set of specifications required for repeatable and reliable long-term explosion monitoring, including thermal stability, reduced recovery time from mass re-centering and large mechanical shocks, sensitivity stability, and transportability. Successful implementation will result in small, hand-held demonstration units with the ability to address national security needs of the DOE/NNSA. Additional applications envisioned include military/defense, scientific instrumentation, oil and gas exploration, inertial navigation, and civil infrastructure monitoring.

## OBJECTIVES

The DOE/NNSA seeks revolutionary sensing innovations for the monitoring of nuclear detonations. Specifically, the performance specifications are to be consistent with those obtainable only by a few elite products available today, but with orders of magnitude reduction in size, weight, power, and cost. The specific sensor specifications solicited are as follows:

- Size – less than 1 in<sup>3</sup>
- Power – less than 100 mW
- Sensor self noise – below USGS NLNM, or approximately 0.5 ng/√Hz
- Dynamic range at least 120 dB over a frequency band of 0.2 to 40 Hz.

In a prior review (Hall, 2008), we summarized basic design considerations for any proposed technology aiming to meet the aforementioned specifications. In particular, it was shown that meeting the noise requirement demands both a) ultra-low thermal mechanical noise from the seismometer proof mass, and b) high resolution displacement measuring capability of the proof mass motion. As an example, a design with a 2 gram proof mass and 50 Hz open loop resonant frequency may be considered. In this case, achieving the required 0.5 ng/√Hz acceleration noise requires a resonance quality factor,  $Q$ , of 100 and an ultra-low displacement resolving capability of 50 fm/√Hz (Hall, 2008). The high resonance  $Q$ , in-turn, requires the use of closed-loop feedback altered dynamics to realize the desired flat frequency response of the sensor. Motivated by this technical discussion, Silicon Audio has proposed design innovations which call upon advanced meso-scale fabrication of mechanical proof-mass elements, photonics-based / motion detection, micro-scale optoelectronic integration, and the integration of closed-loop sensing modalities for high stability and high dynamic range. In prior reviews (Garcia et al., 2009, 2010), several milestones including 1) low noise operation, 2) measured earth-quake recordings, 3) compact (12-oz can size) 3-axis integration, and 4) low power were demonstrated. In subsequent sections, we describe continuing prototype development in these areas as well as next generation innovations already underway.

## Sensor Schematic

The present design, which has undergone rigorous field testing and demonstrates sub 2ng/√Hz noise, is summarized in Figure 1.

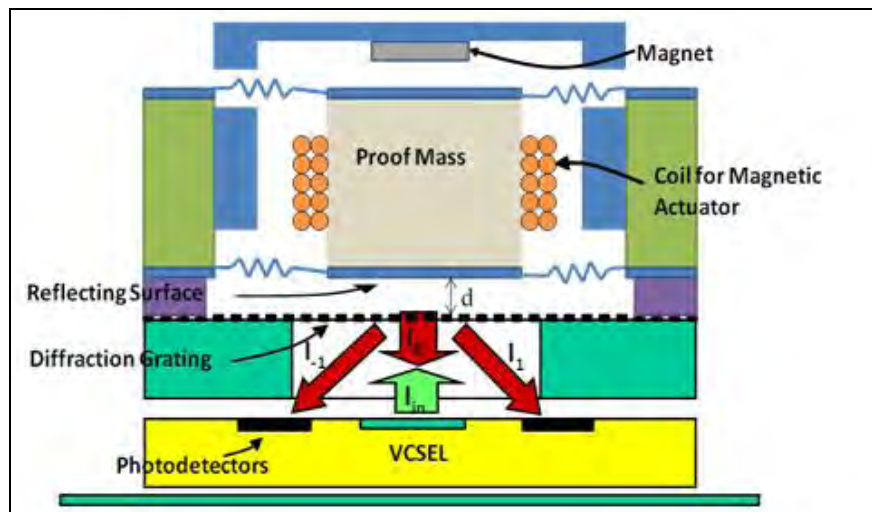


**Figure 1.** Schematic of a photonics based motion detection principle in development. Light from a semiconductor laser such as a vertical cavity surface emitting laser (VCSEL) illuminates a diffraction grating fabricated on silicon. A portion of the incident light reflects directly off of the grating fingers, while the remaining light travels in between the grating fingers and to the proof mass and back to accrue additional phase. A diffracted field results consisting of a zero and higher orders whose angles remain fixed, but whose intensities are modulated by the relative distance between the proof mass and grating with the sensitivity of a Michelson type interferometer.

A sensing method very similar to that summarized in the caption of Figure 1 has been demonstrated and described in detail in prior developments (Lee et al., 2004; Hall et al., 2007; Hall, et al., 2008). The diffraction grating in this system serves the function of an optical beamsplitter, directly reflecting half of the incident light while passing the remaining half to travel to the proof-mass and back to accrue additional phase. Being an optical interference based approach, the displacement resolving capability of the method is of very high fidelity—on the order of  $20 \text{ fm}/\sqrt{\text{Hz}}$  when using small  $500\mu\text{W}$  semiconductor lasers. The intrinsic open loop dynamic range of this approach (i.e., clip level) is limited to approximately  $\lambda/4$ , where  $\lambda$  is the optical wavelength. This corresponds to the peak-to-trough range of an interference cycle (i.e., fringe cycle) and is approximately  $212\text{nm}$  for an  $850\text{nm}$  wavelength semiconductor laser. Considering that  $20\text{fm}$  displacement can be resolved over a  $1 \text{ Hz}$  bandwidth, the intrinsic dynamic range is then  $140\text{dB}$ . Over the  $40\text{Hz}$  measurement bandwidth of interest, the open-loop dynamic range is  $124\text{dB}$ .

It is important that the interferometer be operated at a point of quadrature (i.e., a point of maximum slope and linearity on the interference curve). Figure 2 helps to clarify this by summarizing the theoretically predicted relationship between light intensity of the diffracted beams labeled in Figure 1 vs. the gap distance “d” also labeled in Figure 1. The center beam modulation is complementary to the sum of the exterior beams. Therefore, one can use the difference signal (in practice this is done by simple photocurrent subtraction), as the seismometer output signal. The linear operating region is highlighted in the figure. The slope of this curve is the displacement sensitivity of the detection method (after amplification through a photocurrent-to-voltage amplifier, the unit of the y axis is volts, and the sensitivity is therefore expressed in  $\text{V}/\text{m}$ ).

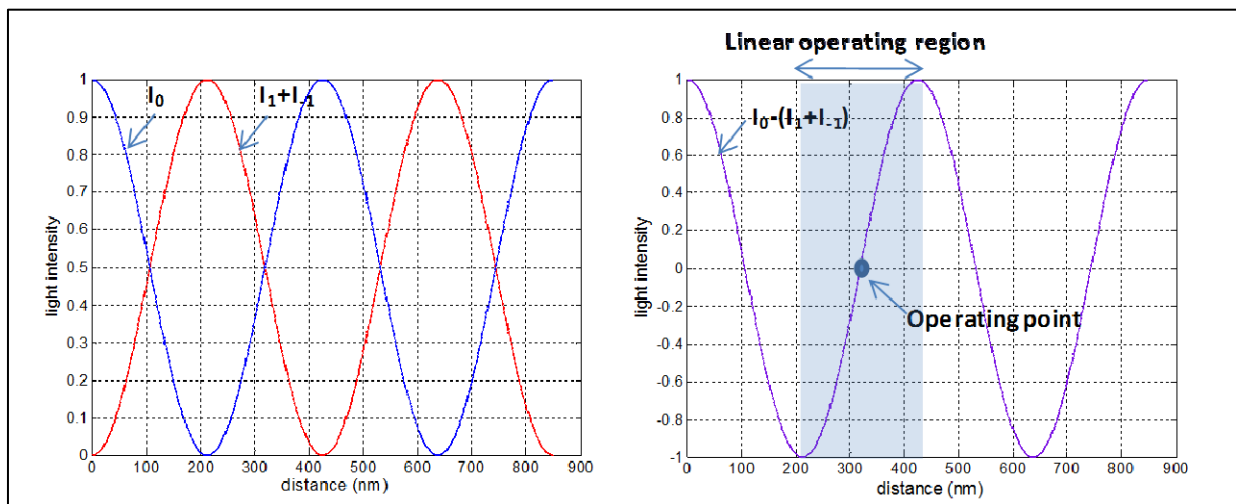


Figure 2. (Left) Theoretically predicted relationship between the diffracted beams labeled in Figure 2 vs. gap distance “d” labeled in Figure 2. (Right) The difference signal is then used to detect the proof mass motion within a single interference fringe.

Operation about a point of quadrature (i.e., the operating point labeled in Figure 2) is maintained by direct actuation of the proof mass using magnetic actuation. In addition, dynamic actuation of the proof mass also enables closed-loop measurement modalities (Liu and Kenny, 2001).

### **RESEARCH ACCOMPLISHED**

In this report we present work related to increasingly miniaturized packaging embodiments and decreased power consumption. We also demonstrate long duration stability of the sensor. The noise performance of these prototypes is consistent with the  $2\text{ng}/\sqrt{\text{Hz}}$  noise floor reported in prior review (Garcia et al., 2010).

### Sensor Prototypes and Field Testing

Silicon Audio has actively pursued the building of sensor prototypes for testing and verification purposes. Figure 3 shows our most recent 3-axis GeoLight prototype. The compact design is roughly the size of a 12-oz can and incorporates a Galperin sensor orientation, automatic mass centering, semi-closed loop force feedback operation, stability features, and sensitivity calibration. Improvements to the mechanical and optical design were based on prior modeling and resulted in a 2x increase in optical sensitivity as well as better alignment tolerance and parameter matching between sensors.

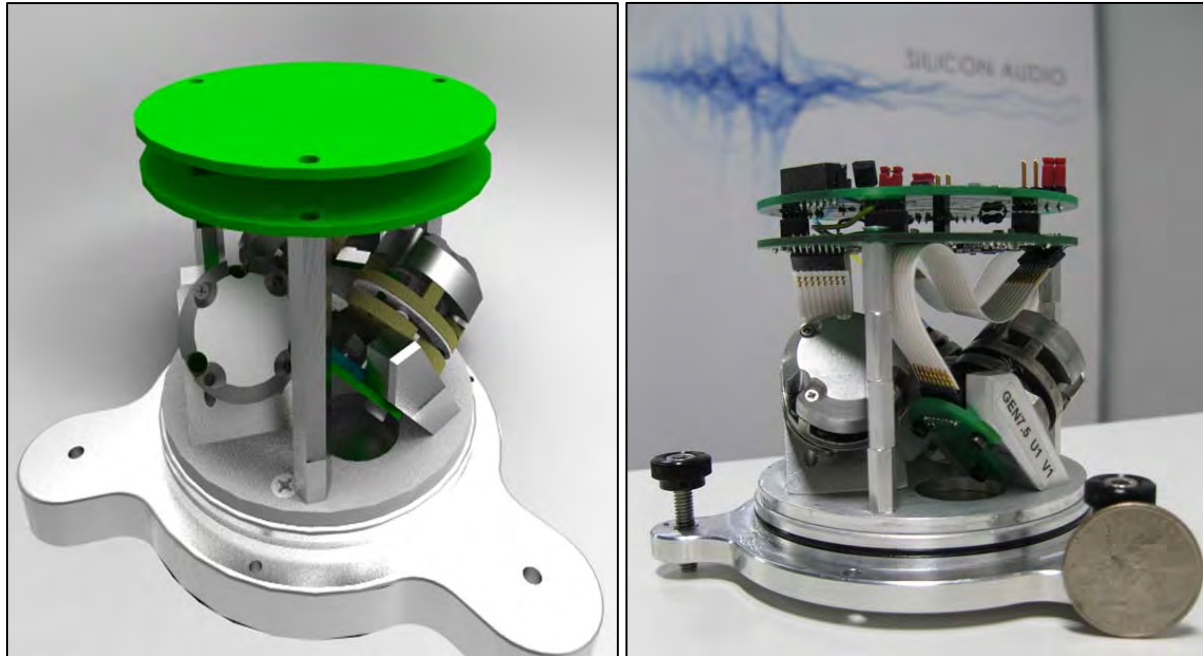


**Figure 3. (left) CAD image showing Silicon Audio's 3-axis design with Galperin sensor orientation. (right) Field tested sensor prototype targeting Class III specifications for broad band seismometers as outlined by the USGS.**

A field test with these sensors has taken place near Austin, TX. This deployment demonstrated 1) continuous operation of all three sensor components during the entire course of the 4 day deployment, 2) recording of microseisms as well as multiple earthquake events, and 3) low power operation. Figure 4 is a time trace of a 24-hour time period in which an earthquake arriving from Nicaragua was recorded. It is important to note that the sensor output is stable throughout the entire test period. A zoomed in view of the Nicaragua earthquake is shown with all three axes plotted in Figure 5. These time traces are consistent with local test stations which also recorded the event, however a reference sensor was not available during this deployment for side-by-side comparison. One final highlight from this field test was the recording of microseisms shown in Figure 6 with a dominant frequency of about 0.25Hz clearly visible after filtering.

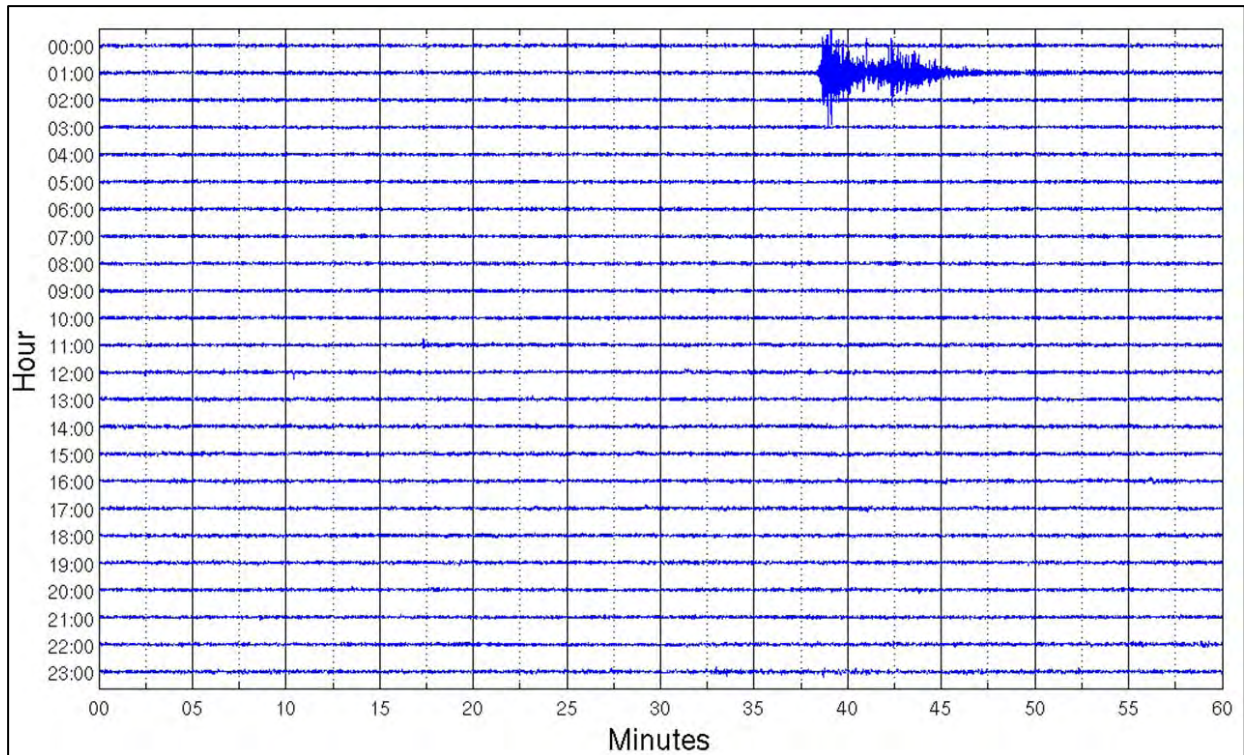


Figure 4. 24-hour recording of a single sensor component demonstrating continual operation of Silicon Audio's GeoLight seismometer prototype. An earthquake arriving from Nicaragua (UTC July 3<sup>rd</sup>, 2011) is visible during the second hour of the recording.

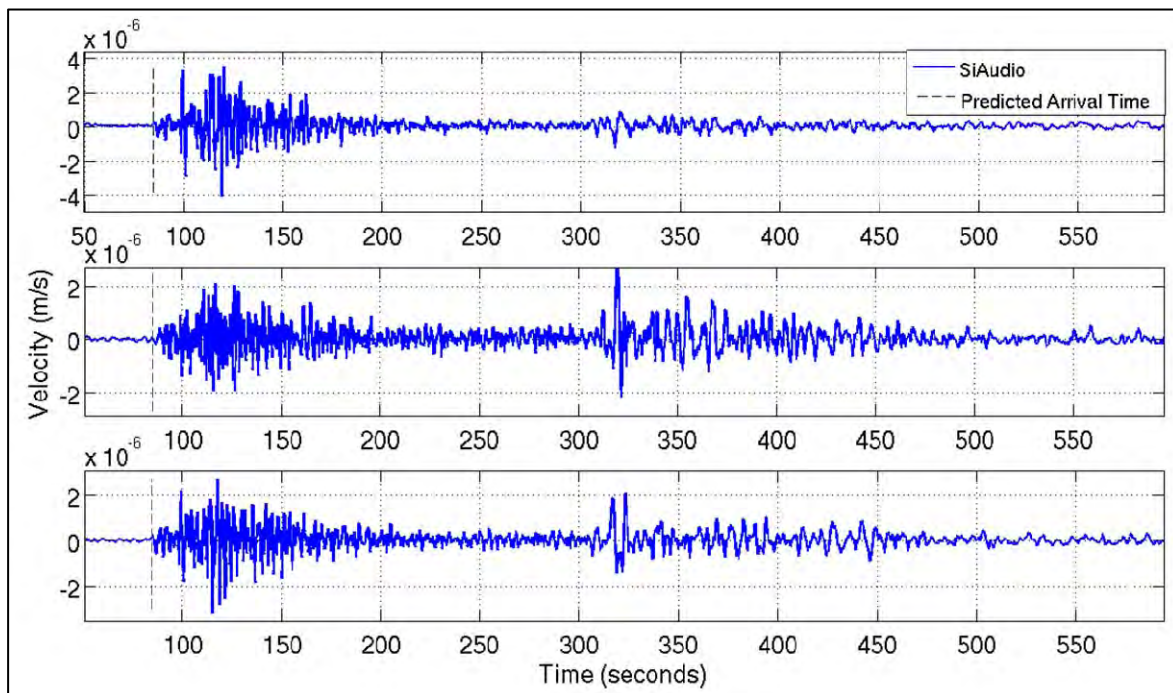


Figure 5. Zoomed-in seismogram of the Nicaraguan earthquake recorded by Silicon Audio's 3-axis GeoLight prototype during a recent field test outside of Austin, TX (UTC event time: July 3<sup>rd</sup>, 2011 – 06:34:40).

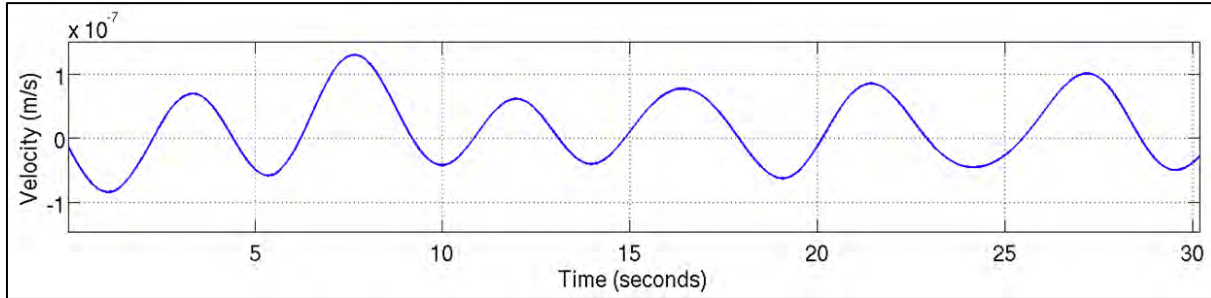


Figure 6. Filtered GeoLight time data showing microseism recordings with peak amplitude at about .25Hz.

*Low Power Operation*

Both optical and electronic system components were selected in order to reduce the power consumption of the 3-axis GeoLight seismometer prototype below the 30mW per axis target. The 3-axis device described in this publication consumes a total of 75mW, meeting the original specification. Figure 7 shows the current draw of the sensor from a 12 V power supply after it has been powered up as well as a rendering of power consumption by function. The laser driver circuit consumes approximately 5.7mW per axis whereas a single VCSEL in continuous operation consumes approximately 4.3mW per axis. Integrated circuit amplifiers draw approximately 5.2mW per axis. Digital control circuitry, high voltage output buffer amplifiers (for ±10 V differential signal outputs), and on-board DC-DC converters consume the majority of the remaining power. Even lower power (down to ~15mW per axis) is possible using more specialized analog circuitry, elimination of the high voltage analog output drivers and pulsed operation of the lasers diodes.

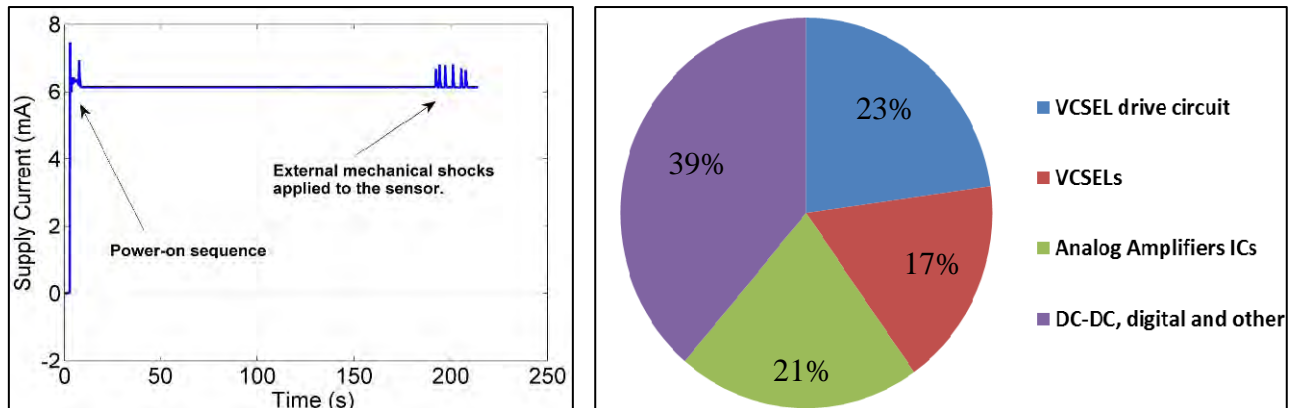


Figure 7. (Left) Current draw using a 12V supply showing power consumption during startup and (right) power consumption by function.

*Alternative Prototype Embodiments*

Other prototyping efforts have demonstrated suitable form factors for both geophone and ocean bottom seismometer (OBS) applications (Figure 8). A significant achievement is the demonstration of a single axis sensor housed within a 1 in<sup>3</sup> geophone package with low power consumption of 19mW. The reduction in power compared with the 3-axis GeoLight prototype can be attributed to absence of high voltage output buffer amplifiers which were unnecessary in this configuration.

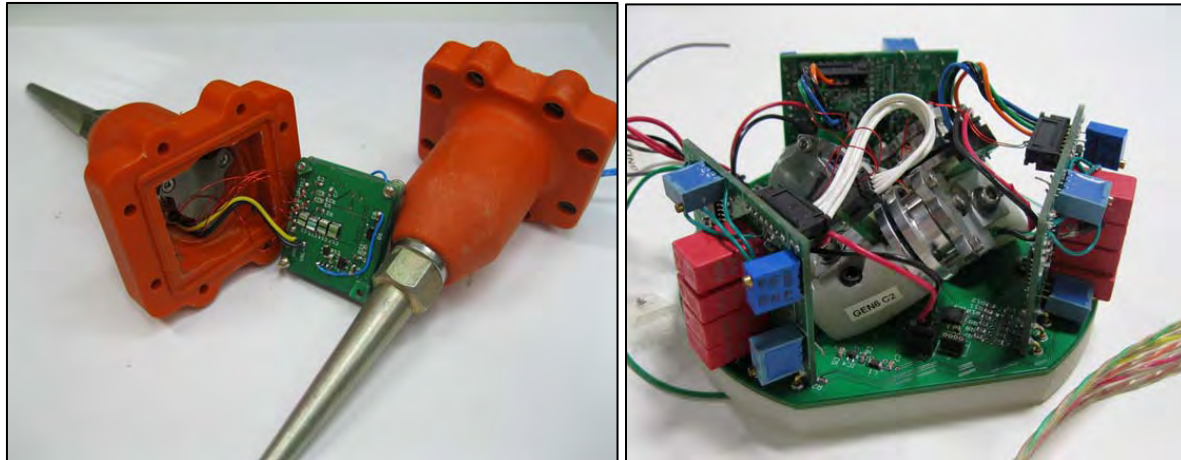


Figure 8. Silicon Audio's optical seismometer packaged as (left) a geophone and as (right) a 3-axis ocean bottom seismometer.

The spring and proof mass structure is a critical component of the seismometer, directly influencing open loop resonances, passband of operation, dynamic range, robustness, noise floor, and shock tolerance. For some strong motion applications, it is desirable to target a sensor with small size, high dynamic range, and high shock tolerance at the expense of a higher noise floor. In such cases, an ideal technology for fabrication of the proof mass structures is silicon micromachining. Silicon as a structural material has many advantages, including high yield strength and high thermal stability. Further, silicon micromachining enables patterning of intricate spring structures difficult to realize with traditional fabrication methods.

We have fabricated silicon structures using the device structure shown below. A silicon-on-insulator (SOI) wafer is used, with the spring structures patterned directly into the thin silicon surface layer (i.e. device layer as labeled in Figure 9). A deep reactive ion etch (DRIE) through the backside of the wafer is used to carve out a cylindrical shaped proof mass 1mm in diameter. The 1 $\mu$ m thick oxide layer serves as an etch stop for the DRIE process and has a high selectivity with respect to silicon. The oxide layer also serves to attach the proof mass to the silicon spring structures. Micrographs of completed proof mass structures are shown in Figure 10.

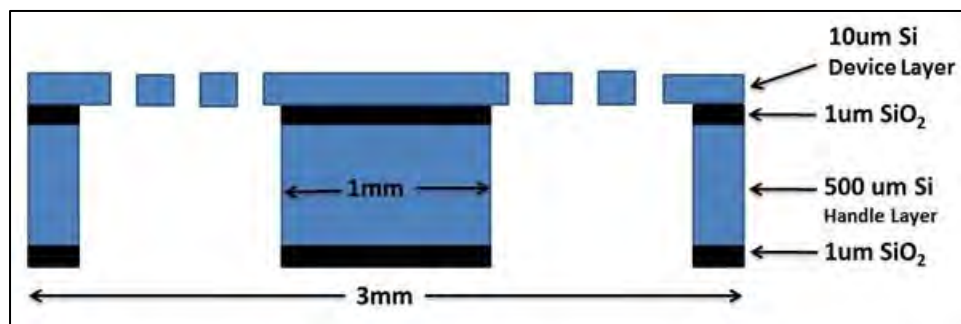
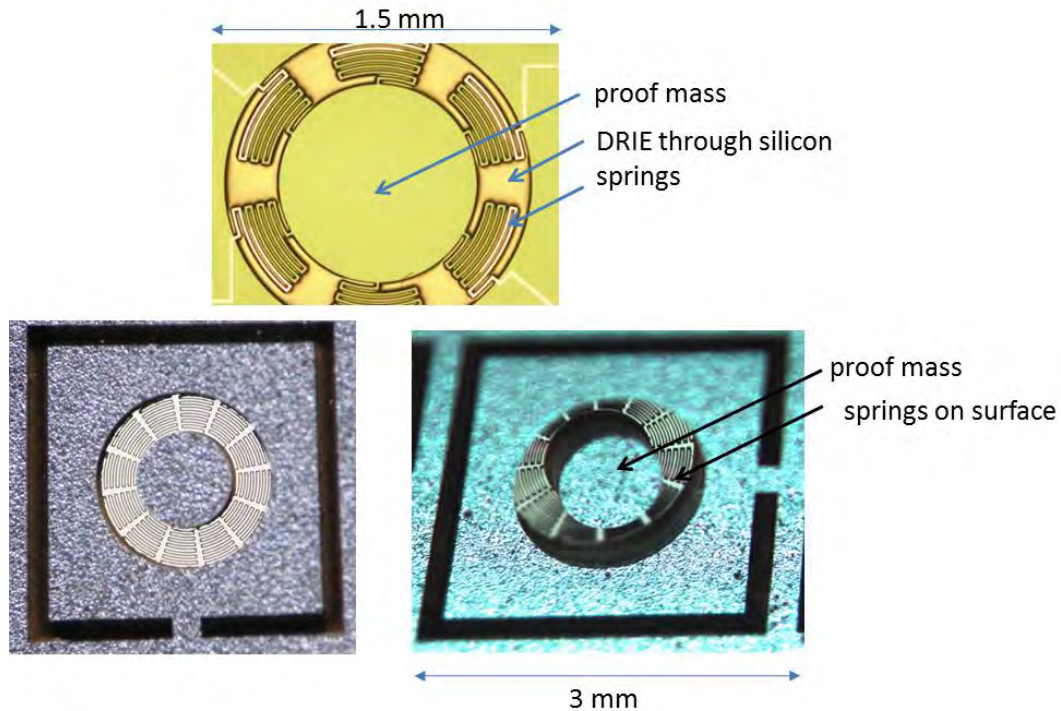


Figure 9. Schematic of strong motion, silicon on insulator (SOI), MEMS structure for ultra-miniature seismic detection.



**Figure 10.** Micrographs of fabricated seismometer proof mass structures in silicon as shown from the topside (top image), backside (bottom-left), and backside isometric view (bottom-right). It should be noted that the top image was captured from a different device than that shown in the bottom 2 images, as can be deduced from the different number of springs.

The proof mass in these designs is approximately  $1\mu\text{gram}$ , and the resonant frequency of the fabricated structures ranges from 100Hz – 1 kHz. Assuming an open loop  $Q$  of 100 can be achieved, the corresponding calculated thermal-mechanical noise floors for these designs ranges from  $32\text{ ng}/\sqrt{\text{Hz}}$  to  $100\text{ ng}/\sqrt{\text{Hz}}$ , respectively. These sensors open up the possibility for extremely small, MEMS-scale, surface-mountable units. Their packaging and characterization is the subject of future work.

### CONCLUSIONS AND RECOMMENDATIONS

Silicon Audio is addressing the NNSA’s rigorous seismometer specifications using an approach that combines silicon micromachined optical elements, integrated semiconductor lasers, photo detection electronics, and meso-scale proof mass structures. This review article focused on a grating based implementation and significant accomplishments were discussed including , demonstration of stable 3-axis prototypes and parallel efforts addressing ultra-miniature architectures. Future developments will continue to focus on improved noise performance in the 100mHz-3Hz band as well as miniaturization efforts which are already underway. We envision complete units integrated into a 3-axis sensor package roughly the size of a 9-volt battery.

### ACKNOWLEDGEMENTS

We thank the University of Texas’ Institute of Geophysics for assistance with Phase I and Phase II field test demonstrations.

### REFERENCES

Hall, N. A. (2008). Micro-seismometers via advanced mesoscale fabrication, in *Proceedings of the 30<sup>th</sup> Monitoring Research Review: Ground-Based Nuclear Explosion Monitoring Technologies*, LA-UR-08-05261, Vol. 1, pp. 610–614.

## 2011 Monitoring Research Review: Ground-Based Nuclear Explosion Monitoring Technologies

- Hall, N. A., M. Okandan, R. Littrell, B. Bicen, and F. L. Degertekin (2007). Micromachined optical microphones with low thermal-mechanical noise levels, *J. Acous. Soc. Am.* 122 (4): 2031–2037.
- Hall, N. A., M. Okandan, R. Littrell, D. K. Serkland, G. A. Keeler, and K. Peterson (2008). Micromachined accelerometers with optical interferometric read-out and integrated electrostatic actuation, *J. Microelectromech. Syst.* 17 (1): 37–44.
- Hobbs, P. C. D. (1997). Ultrasensitive laser measurements without tears, *Applied Optics* 36: (4), 903–920.
- Lee, W., N. A. Hall, et al. (2004). Fabrication and characterization of a micromachined acoustic sensor with integrated optical readout. *IEEE Journal on Selected Topics in Quantum Electronics* 10: (3), 643–651.
- Liu, C. H. and T. W. Kenny (2001). A high-precision, wide-bandwidth micromachined tunneling accelerometer, *J. Microelectromech. Syst.* 10: (3), 425–433.
- Garcia, C. T., Onaran, G., Avenson, B., Ellis, M., and N. A. Hall (2009). Micro-Seismometers via Advanced Mesoscale Fabrication. in *Proceedings of the 2009 Monitoring Research Review: Ground-Based Nuclear Explosion Monitoring Technologies*, LA-UR-09-05276, Vol. 1, pp. 330–337.
- Garcia, C.T., Onaran, G., Avenson, B., Yocom, B., and N. A. Hall (2010). Micro-Seismometers via Advanced Mesoscale Fabrication. in *Proceedings of the 2010 Monitoring Research Review: Ground-Based Nuclear Explosion Monitoring Technologies*, , LA-UR-10-05578, Vol. 1, pp. 280–288.